JOURNAL OF MATERIALS SCIENCE 11 (1976) 696–702

Crystallite size distribution and lattice distortions in uniaxially drawn polyethylene

OSAMU YODA, NAOYUKI TAMURA
Takasaki Research Establishment, Japan Atomic Energy Research Institute, Takasaki, Gunma, Japan

KENJI DOI
Tokai Research Establishment, Japan Atomic Energy Research Institute, Ibaraki, Japan

Crystallite size distributions and lattice distortions in the lateral direction as well as in the chain direction of uniaxially drawn polyethylene are analysed from 1 1 0 and 0 0 2 Debye–Scherrer line profiles by means of a Fourier technique. The size distribution in the [1 1 0] direction of the original (undrawn) sample consists of two well-defined components having maxima at 220 and 310 Å. In this lateral direction, crystallites break up into smaller units by drawing in such a way that each component in the original size distribution has its own scheme of degradation. In the chain direction [0 0 1] a similar mechanism of crystallite reconstitution is possibly operating, although the size distribution of the original sample in this direction could not be obtained. Lattice distortions in the drawn samples are of the strained-lattice type, except for the case of cold-drawing in the lateral direction [1 1 0]. [1 1 0] distortions in the cold-drawn specimen can be regarded as paracrystalline distortion. In this case, the strength of paracrystalline distortion is estimated as about one-half of the value given by Hosemann for similar polyethylene samples.

1. Introduction

The change in the crystallite size produced by the deformation process, e.g. drawing or rolling, has been extensively investigated by many authors. Their interests, however, have been usually confined within the mean size as obtained by the analyses of X-ray diffraction patterns (e.g. [1]) or thermal diagrams (e.g. [2]).

In the present investigation Fourier analyses of line profiles are made for 1 1 0 and 0 0 2 profiles of cold-drawn and hot-drawn polyethylene films, with a view to obtaining changes in crystallite size and lattice distortions in the lateral and the chain directions due to uniaxial drawing.

2. Experimental

2.1. Sample preparation

The measurements were made on unfractionated, additive-free samples of Sholex 6050 (Japan Olefin Chem.). This is a linear polyethylene made by Phillips' method and has a viscosity-averaged molecular weight $M_v = 5 \times 10^4$. Samples were pressed and moulded from the melt at 160° C and subsequently quenched in water. The quenched films were cut into narrow strips and drawn at a rate of 1 cm min^{-1} at 20° C (cold-drawn) and 100° C (hot-drawn) with a draw ratio of $\lambda \simeq 10$. In the latter case, the sample was annealed at 110° C for 10 min and cooling to room temperature took place without tension.

The degree of crystallinity was determined by wide-angle nmr measurements.

2.2. Profile measurement

Monochromatic Cu$K\alpha_1$ rays were generated with the aid of a Johansson-type curved-crystal monochromater, which was inserted between the X-ray tube and the divergence slit of the diffractometer. A scintillation counter was used as a detector with a pulse-height analyser.

1 1 0 profiles of original (undrawn) and drawn polyethylene, and 0 0 2 of drawn specimens were

recorded by the step-scanning method. Throughout the measurements, the step width in 2θ was fixed to 0.02°. All profiles were observed in transmission arrangement.

The observed profiles were corrected for the instrumental broadening by means of Stokes's method [3] using well-crystallized graphite powder as a standard substance. The 0 0 2 profile of graphite ($2\theta \simeq 26.5°$) was adopted to correct 1 1 0 profiles of polyethylene specimens ($2\theta \simeq 21.5°$), and 1 1 0 of graphite ($2\theta \simeq 77.5°$) to correct the 0 0 2 profile of polyethylene ($2\theta \simeq 74.5°$). Fig. 1 shows the observed profiles of the 1 1 0 and 0 0 2 reflections. First, the amorphous background in the neighbourhood of the 1 1 0 profile was subtracted by hand, as a smooth curve passing through the tails of the 1 1 0 and adjacent 2 0 0 profiles (dotted line in Fig. 1a), after eliminating the circuit noises. The intensity data were then processed for background estimation so that the variance range function [4] became linear. The resultant background was indicated by a solid line in the figure. For the 0 0 2 profile, the amorphous component was approximated by a straight line passing through the intensity at 70° and 80° of 2θ (dotted line in Fig. 1b). The variance range function method was then applied, giving the background as shown by the solid line in Fig. 1b. Other corrections, such as Lorentz-polarization and absorption, were found unnecessary because of the narrowness of the profiles. Data processings and calculations were carried out by HP 2100A with a FORTRAN program written by O.Y.

3. Method of analysis

The method of analysis employed here is based on that developed by one of the present authors [5], and applied to the 1 1 0 profiles of polyethylenes of various origins [6].

Let us consider a Debye–Scherrer line from a reflecting plane $(h\,k\,l)$. All the crystallites may then be regarded as constituted from linear structures $\rho_n(x)$'s, $\rho_n(x)$ being the projection of the structure of the nth crystallite $\rho_n(x)$ onto a line perpendicular to the reflecting plane $(h\,k\,l)$†.

The profile of the $h\,k\,l$ reflection, $I(s)$, is expressed as:

$$I(s) = \sum_{1}^{N} |A_n(s)|^2 \equiv N|A_0(s)|^2, \qquad (1)$$

where $A_n(s)$ is the Fourier transform of $\rho_n(x)$. The second half of Equation 1 defines the function $A_0(s)$ whose Fourier transform gives the unfolded structure $\rho_0(x)$ of the averaged convolution [5]. Let Equation 1 be Fourier-transformed:

$$V(x) = \sum_{1}^{N} \{\rho_n(x) * \rho_n(x)\} = N\{\rho_0(x) * \rho_0(x)\} \qquad (2)$$

with the symbol * standing for the convolution product. Although the structure $\rho_0(x)$ can hardly claim realistic significance, its self-convolution, $V(x)$ of Equation 2, represents the statistics of the correlation between atoms in the direction perpendicular to $(h\,k\,l)$.

The method [5] constitutes deriving the structure $\rho_0(x)$ from the Fourier transform of the square root of $I(s)$, and constructing from this the correlation statistics $V(x)$ via Equation 2. If $\rho_0(x)$ is assumed as a linear arrangement of point atoms:

$$\rho_0(x) = \sum_{m} \delta(x - ma_{hkl} - \epsilon_m)\, p(m), \qquad (3)$$

where $p(m)$ measures atomic density at $ma_{hkl} + \epsilon_m$, a_{hkl} and ϵ_m being the mean lattice spacing and the deviation of the mth atom from the mth lattice point, respectively.

Once the structure $\rho_0(x)$ and its self-convolution $V(x)$ are obtained, the number-fraction $g(M)/M$ of the linear structure with the length Ma_{hkl} is given:

$$\begin{aligned} g(M)/M &= \Delta V(Ma_{hkl}) - \Delta V((M+1)a_{hkl}) \\ \Delta V(Ma_{hkl}) &= V((M-1)a_{hkl}) - V(Ma_{hkl}). \end{aligned} \qquad (4)$$

The lattice distortions, or the fluctuations in lattice spacings, defined as the square-roots of the second moments of $(\epsilon_m - \epsilon_{m'})$'s are given by [6]

$$\Delta(n) \equiv \Delta(m-m') = \left\{ \frac{\sum\sum_{m\,m'} p(m)p(m')(\epsilon_m - \epsilon_{m'})^2}{\sum\sum_{m\,m'} p(m)p(m')} \right\}^{\frac{1}{2}}. \qquad (5)$$

As the structure $\rho_0(x)$ derived from the profile can furnish all the quantities appearing on the right-hand side of Equation 5 (see Equation 3), it permits the derivation of the lattice distortions without knowing *a priori* the nature of distortions, namely paracrystalline or strained-lattice [6].

† For the precise definition of $\rho_n(x)$, see the appendix of [5].

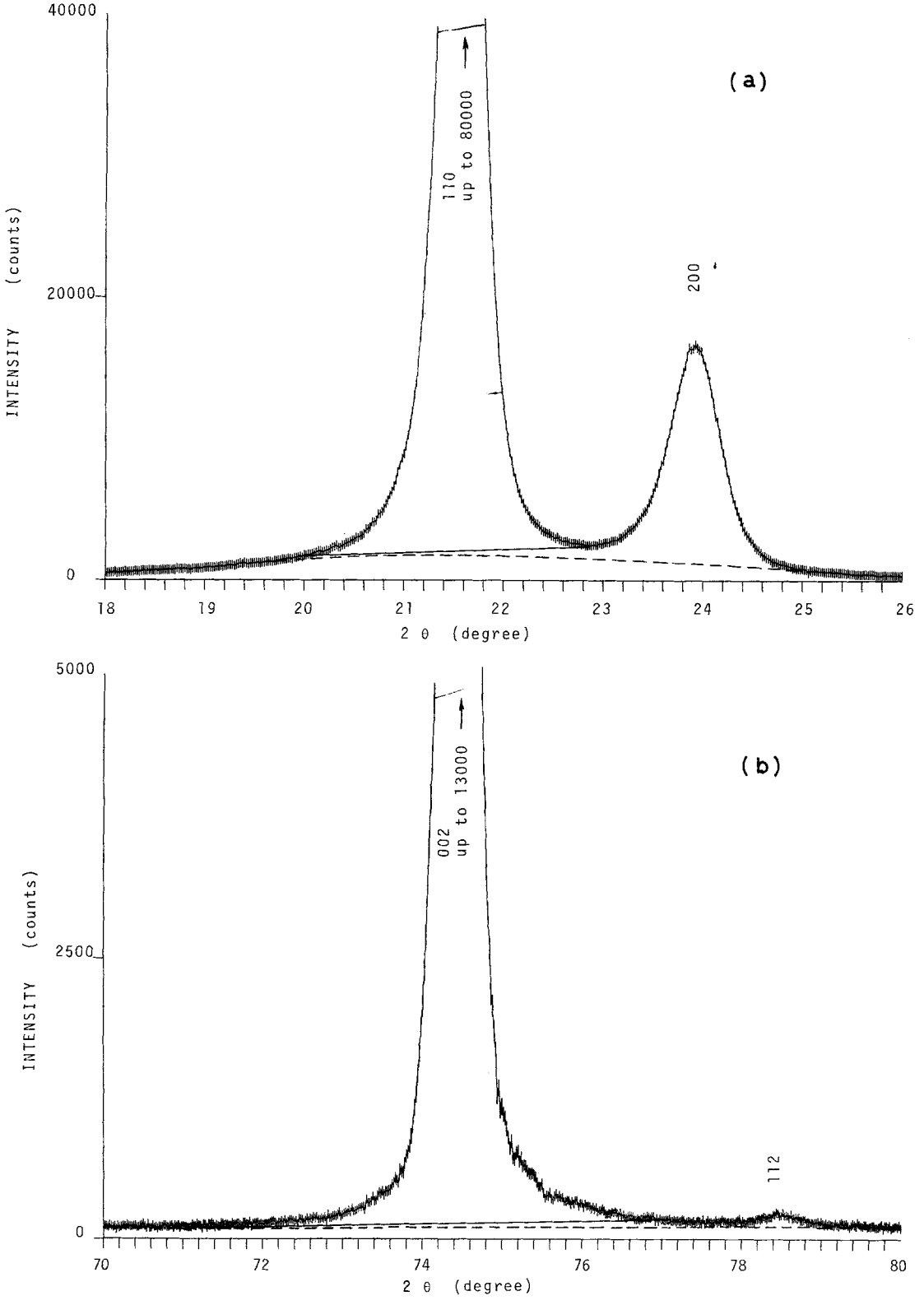

Figure 1 Background estimations of hot-drawn samples. In the neighbourhood of (a) 1 1 0 and (b) 0 0 2 profiles, dotted lines indicate the amorphous components approximated by a smooth curve in (a) and a straight line in (b). Solid lines give the background levels estimated by the variance range function method. Ordinates of the profiles designate statistical errors.

TABLE I Parameters specifying the profile

Profile	Lattice spacing (Å)	Integral breadth ($Å^{-1}$)	Weighted-mean size (Å)
Original 1 1 0	4.13	0.0033	280
Cold-drawn 1 1 0	4.14	0.0085	90
Hot-drawn 1 1 0	4.12	0.0051	170
Cold-drawn 0 0 2	1.272	0.0064	125
Hot-drawn 0 0 2	1.273	0.0046	210

4. Results and discussion

4.1. Crystallite size distribution

Distribution curves of crystallite sizes are shown in Fig. 2 for the [1 1 0] direction, and in Fig. 3 for the [0 0 1] direction of drawn samples. In those figures, weighted-mean sizes calculated from the size distribution function are marked by arrows. In Table I the lattice spacing, Stokes-corrected integral breadth, and the weighted-mean size for each profile are given.

4.1.1. Change in the crystallite size distribution in the lateral direction

In the original (undrawn) sample, the lateral crystallite size distribution is peaked around 220 and 310 Å (see Fig. 2a). Crystallites smaller than 200 Å are hardly observed in this sample. This is quite similar to the crystal mats as shown in our preceding work (cf. Fig. 5 of [6]).

Two distinct peaks at 220 and 310 Å disappear by cold-drawing with the draw-ratio of 10 (Fig. 2b); crystallites being broken up into smaller sizes. There are no crystallites larger than 150 Å, and the maximum frequency in the crystallite size distribution appears below 60 Å.

With hot-drawing, crystallites having sizes of 220 and 310 Å are still present to some extent, but most of the crystallites decompose into smaller units, namely those of 95 and 160 Å in size (Fig. 2c). These results show that in the hot-drawn sample, polymer chains are able to re-arrange themselves into crystallites of smaller sizes. In the cold-drawn sample, however, the lack of sufficient chain mobility results in the breakup of the crystallites into much smaller units by external force.

Peak positions and peak areas in the size distribution given in Figs. 2 and 3 are summarized in

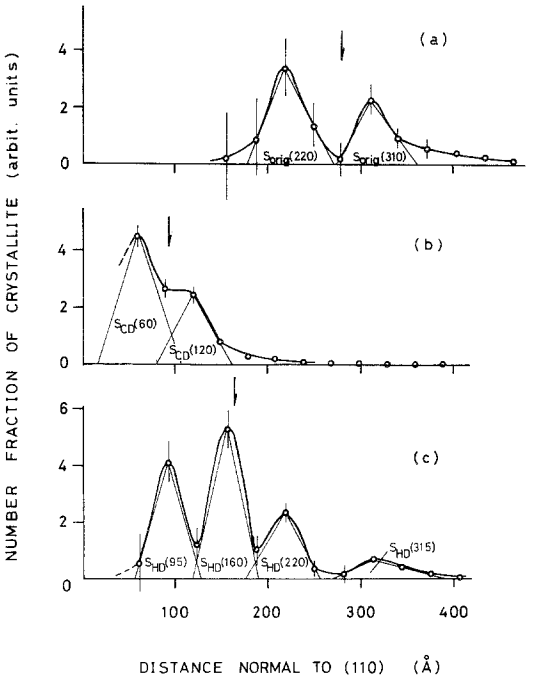

Figure 2 Crystallite size distributions in the lateral direction. (a) original; (b) cold-drawn; and (c) hot-drawn samples. The arrow shows the position of the weighted-mean size. S_{orig} (220), for example, means the area of the peak at 220 Å in the original sample, approximated by a triangle.

Table II. Inspection of the curves in Figs. 2a, b and c may reveal that a rule exists which governs the degradation of crystallites with drawing. Let the areas of peaks at 220 and 310 Å in Fig. 2a be $S_{orig}(220)$ and $S_{orig}(310)$, respectively. Similarly peaks in Fig. 2b are denoted as $S_{CD}(60)$ and $S_{CD}(120)$, and peaks in Fig. 2c as $S_{HD}(95)$, $S_{HD}(160)$, $S_{HD}(220)$ and $S_{HD}(315)$. It is then found that

$$\frac{S_{orig}(220) \times 220}{S_{orig}(310) \times 310} = 0.89$$

$$\frac{S_{CD}(60) \times 60}{S_{CD}(120) \times 120} = 0.90(6)$$

$$\frac{S_{HD}(95) \times 95 + S_{HD}(220) \times 220}{S_{HD}(160) \times 160 + S_{HD}(315) \times 315} = 0.99$$

that is, the ratios defined in the left-hand side of the above equations are found equal within estimated errors. On the other hand, the total mass of crystallites (crystallinity) is nearly conserved before and after drawing (see Table II). If we assume that the density of the crystallites is

TABLE II Assignment of the peaks in the size distribution curve

	Peak	Original		Cold-drawn		Hot-drawn	
		Size (Å)	Number of crystallites*	Size (Å)	Number of crystallites*	Size (Å)	Number of crystallites*
[1 1 0]	I			60	3.4	95	2.7
	II			120	1.9	160	3.7
Direction	III	220	2.9			220	2.4
	IV	310	2.3			315	0.6
[0 0 1]	I			90	5.9	160	3.6
	II			150	3.2	220	2.5
Direction	III			210	0.7	280	1.6
	IV			300	0.3	340	1.1
Crystallinity†		≃ 80%		≃ 83%		≃ 85%	

*The area of the triangle in an arbitrary unit (see Figs. 2 and 3).
† Determined by wide-angle nmr.

not affected by drawing, then the above relations suggest a possible scheme of degradation as follows:

cold-drawing:

$$\begin{aligned} \text{cryst}_{\text{orig}}(220) &\longrightarrow \text{cryst}_{\text{CD}}(60) \\ \text{cryst}_{\text{orig}}(310) &\longrightarrow \text{cryst}_{\text{CD}}(120); \end{aligned} \tag{7}$$

hot drawing:

$$\begin{aligned} \text{cryst}_{\text{orig}}(220) &\longrightarrow \text{cryst}_{\text{HD}}(220) \\ &\searrow \text{cryst}_{\text{HD}}(95) \\ \text{cryst}_{\text{orig}}(310) &\longrightarrow \text{cryst}_{\text{HD}}(310) \\ &\searrow \text{cryst}_{\text{HD}}(160), \end{aligned} \tag{8}$$

where $\text{cryst}_{\text{orig}}(220)$, for example, means the crystallite in the original sample with size of 220 Å in the direction perpendicular to the chain direction.

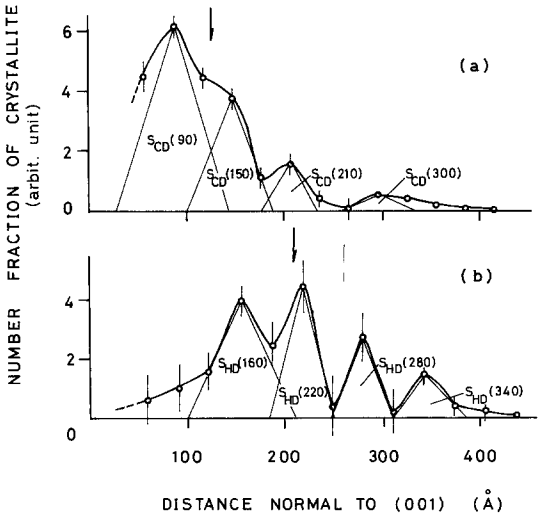

Figure 3 Crystallite size distributions in the chain direction. (a) cold-drawn; and (b) hot-drawn samples.

The above scheme implies that each component in the size distribution in the original film has its own scheme of degradation which is independent of that of the other component.

4.1.2. Crystallite size distribution in the chain direction

The shape of the distribution curves of crystallite sizes in the chain direction after cold- and hot-drawing are similar to those in the lateral direction, although the peak positions are slightly displaced outwards (Fig. 3, Table II). By drawing at room temperature (cold-drawing), most of the crystallites are smaller than 150 Å in size, while small distributions still remain at 210 and 300 Å (Fig. 3a).

With the same notation as adopted in the preceding section, the following relations are observed in the distribution functions of Fig. 3:

$$\begin{aligned} \frac{S_{\text{CD}}(90) \times 90 + S_{\text{CD}}(210) \times 210}{S_{\text{CD}}(150) \times 150 + S_{\text{CD}}(300) \times 300} &= 1.2 \\ \frac{S_{\text{HD}}(160) \times 160 + S_{\text{HD}}(280) \times 280}{S_{\text{HD}}(220) \times 220 + S_{\text{HD}}(340) \times 340} &= 1.1, \end{aligned} \tag{9}$$

i.e. the ratios on the left-hand side are equal; this is similar to the relation found in the preceding section. Equation 9 refers only to drawn samples, the 0 0 2 reflection of the undrawn samples not being detected. It is seen, however, that Equation 9 corresponds to the second and third lines of Equation 6, which means that in the [0 0 1] direction relations between the com-

ponents in drawn samples are quite similar to those in the [1 1 0] direction. One might suppose, therefore, that a relation corresponding to the first line of Equation 6 exists in the [0 0 1] direction, thus the degradation scheme analogous to Equations 7 and 8 is operating in the chain direction as well.

In a recent report [7], polydispersive crystallite size distributions are also found in the molecular chain direction of annealed polyethylene single crystals.

4.2. Lattice distortions

Observed lattice distortions of the samples are shown in Figs. 4 and 5 for the [1 1 0] and [0 0 1] directions, respectively. A noticeable change is also induced in the lattice distortions with the temperature of drawing.

The nature of observed lattice distortions (Δ in Equation 5) were examined, namely whether they were of strained-lattice or paracrystalline type distortions. The strained-lattice distortion is defined as

$$\Delta_s(x) = \alpha x, \tag{10}$$

while the paracrystalline distortion is, with a lack of long-range order,

$$\Delta_p(x) = \beta x^{1/2}, \tag{11}$$

with $x = na_{hkl}(n = 0, 1, 2,...)$, and α and β are constants [8].

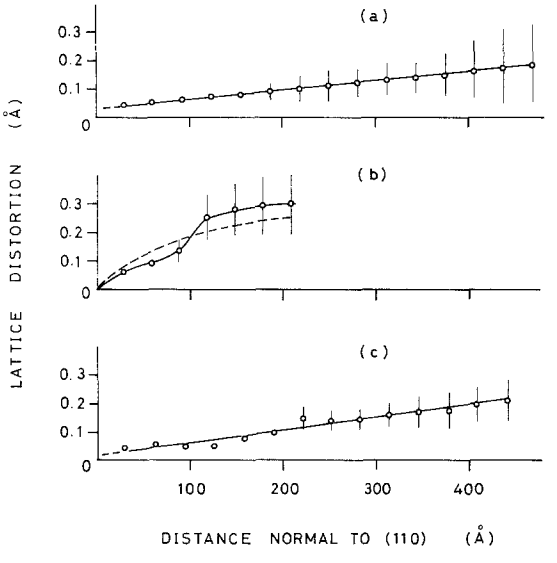

Figure 4 Lattice distortions in the lateral direction. (a) original; (b) cold-drawn; and (c) hot-drawn samples. (b) can be regarded as a parabola as indicated by the dotted line.

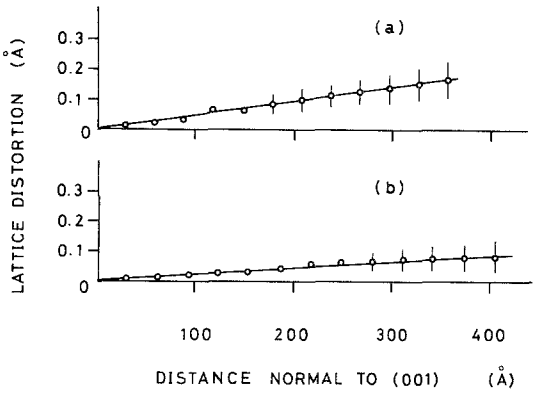

Figure 5 Lattice distortions in the chain direction. (a) cold-drawn; and (b) hot-drawn samples.

[1 1 0] distortion in the original film is rather small and proves to be of the strained-lattice type. In the cold-drawn sample, lattice distortions are larger than those in the original material by a factor of two at the shortest distance, and are of the paracrystalline nature within experimental error; they are attributed to the large deformation and the lack of sufficient mobility. This situation is consistent with the fact that throughout the deformation process the lattice spacing increases slightly (see Table I). On the other hand, distortions in the hot-drawn sample are similar both in degree and in type to those in the original film which was obtained from the melt, since sufficient mobility permits the relaxation of polymer chains in the course of drawing. Same lattice spacings of the original and hot-drawn films (Table I) support this interpretation.

The strength of paracrystalline distortion g defined by Hosemann [8] as

$$g = \Delta a_{hkl}/a_{hkl}, \tag{12}$$

can be estimated from Fig. 3b. a_{hkl} and Δa_{hkl} in Equation 12 are the average $(h\,k\,l)$ lattice spacing and the variation of lattice spacings, respectively.

The curve in Fig. 3b can be approximated by a parabola, as shown by the dotted curve, from which the value of g is derived as follows: the paracrystalline distortion $\Delta_p(na_{hkl})$ is related to Δa_{hkl} by [9]

$$\Delta_p(na_{hkl}) = \sqrt{n} \cdot \Delta a_{hkl}, \tag{13}$$

g is then written as

$$g = \Delta a_{hkl}/a_{hkl} = \Delta_p(na_{hkl})/\sqrt{n} \cdot a_{hkl} \tag{14}$$

From Fig. 3b, g is then found to be 0.90% with

$\Delta_p = 0.18$ Å at $na_{hkl} = 100$ Å, which is almost one-half of the value given by Hosemann [9] for similar polyethylene samples.

In the chain direction, distortions are of the long-range nature in the cold-drawn, as well as in the hot-drawn cases, which seems consistent with the crystal structure of this material where atoms are more tightly bound in the chain direction than in the lateral direction. Nevertheless, the cold-drawn lattices are distorted about twice as much as the hot-drawn lattices.

Acknowledgement

The authors would like to thank Dr I. Kuriyama for his interest and discussion. Their thanks are also due to Mr N. Hayakawa for the measurements of wide-angle nmr.

References

1. W. GLENZ and A. PETERLIN, *J. Polymer Sci. A-2,* **9** (1971) 1243.
2. G. MEINEL, N. MOROSOFF and A. PETERLIN, *ibid* **8** (1970) 1723.
3. A. R. STOKES, *Proc. Phys. Soc. Lond.* **61** (1948) 382.
4. J. I. LANGFORD and A. J. C. WILSON "Crystallography and Crystal Perfection" (Academic Press, London, 1963).
5. K. DOI, *Acta Cryst.* **14** (1961) 830.
6. O. YODA, K. DOI, N. TAMURA and I. KURIYAMA, *J. Appl. Phys.* **44** (1973) 2211.
7. A. H. WINDLE, *J. Mater. Sci.* **10** (1975) 1959.
8. R. HOSEMANN and S. N. BAGCHI, "Direct Analysis of Diffraction by Matter" (North Holland, Amsterdam, 1962).
9. R. HOSEMANN, *J. Polymer Sci.* **C20** (1967) 1.

Received 9 July and accepted 6 October 1975.